PAPER

Check for updates

Broadening spectral responses and achieving environmental stability in SnS2/Ag-NPs/HfO2 flexible phototransistors†

Muhammad Farooq Khan, [iD] ‡[a] Sana Sadaqat,‡[b] Muhammad Asghar Khan,‡[c] Shania Rehman, [iD] [d] Waqas Siddique Subhani,[e] Mohamed Ouladsmane,[f] Malik Abdul Rehman,[g] Fida Ali, [iD] [h] Harri Lipsanen, [iD] [h] Zhipei Sun, [iD] [h] Jonghwa Eom [iD] *[c] and Faisal Ahmed [iD] *[h]

Layered two-dimensional (2D) materials have gained popularity thanks to their atomically thin physique and strong coupling with light. Here, we investigated a wide band gap (≥ 2 eV) 2D material, *i.e.*, tin disulfide (SnS2), and decorated it with silver nanoparticles, Ag-NPs, for broadband photodetection. Our results show that the SnS2/Ag-NPs devices exhibit broadband photodetection ranging from the ultraviolet to near-infrared (250–1050 nm) spectrum with decreased rise/decay times from 8/20 s to 7/16 s under 250 nm wavelength light compared to the bare SnS2 device. This is attributed to the localized surface plasmon resonance effect and the wide band gap of SnS2 crystal. Furthermore, the HfO2-passivated SnS2/Ag-NPs devices exhibited high photodetection performance in terms of photoresponsivity ($\sim$12 500 A W^{-1}), and external quantum efficiency ($\sim$6 $\times$ 10^6%), which are significantly higher compared to those of bare SnS2. Importantly, after HfO2 passivation, the SnS2/Ag-NPs photodetector maintained the stable performance for several weeks with merely $\sim$5.7% reduction in photoresponsivity. Lastly, we fabricated a flexible SnS2/Ag-NPs photodetector, which shows excellent and stable performance under various bending curvatures (0, 20, and 10 mm), as it retains $\sim$80% of its photoresponsivity up to 500 bending cycles. Thus, our study provides a simple route to realize broadband and stable photoactivity in flexible 2D material-based devices.

1. Introduction

Photodetectors are sensors that convert incident photons into electrical signals.[1] The energies of the incident photons may span throughout the electromagnetic spectrum ranging from X-ray, ultraviolet (UV), visible, and infrared (IR) to the terahertz range for different applications.[2,3] Commercially, silicon-based photodetectors are dominant in the visible to near-IR spectrum due to their small band gap (1.1 eV) and Earth abundance.[4] UV detection is realized either by coupling silicon photodetectors with appropriate filters or replacing Si with wide band gap semiconductors such as GaN, AlN and SiC and bulk heterostructures.[5–7] These techniques pose fabrication complexities and limit the miniaturization of photodetectors to meet the criteria for future scaled devices. UV detection is important in space sciences for satellite communication, in the healthcare field for biological imaging and disinfection of bio-agents, and in various chemical analyses and water purification fields.[8–11]

Semiconducting two-dimensional (2D) materials are advantageous to bulk semiconductors for photodetection because of their atomically thin and flexible nature, dangling bond-free surfaces, and wide range of energy gaps covering the UV to mid-IR spectrum.[12] Previously, most efforts have been dedicated towards visible and IR photodetection since majority of well-studied 2D semiconductors such as MoS2, WSe2, and black phosphorus possess energy gaps < 2 eV.[13] Here, we inves-

[a]*Department of Electrical Engineering, Sejong University, Seoul 05006, Republic of Korea*

[b]*Department of Physics, Riphah International University, Faisalabad Campus, 44000, Pakistan*

[c]*Department of Physics and Astronomy, Sejong University, Seoul 05006, Republic of Korea. E-mail: eom@sejong.ac.kr*

[d]*Department of Semiconductor System Engineering, Sejong University, Seoul 05006, Republic of Korea*

[e]*Department of Physics, University of Lahore, Lahore, 53700, Pakistan*

[f]*Department of Chemistry, College of Science, King Saud University, Riyadh, 11451, Saudi Arabia*

[g]*Department of Chemical Engineering, New Uzbekistan University, Tashkent, 100007, Uzbekistan*

[h]*Department of Electronics and Nano Engineering, Aalto University, P.O. Box 13500, FI-00076 Aalto, Finland. E-mail: faisal.ahmed@aalto.fi*

†Electronic supplementary information (ESI) available. See DOI: https://doi.org/10.1039/d3nr04626e

‡These authors contributed equally to this work.

tigate the broadband UV-visible-near IR photodetection based on wide bandgap (2–2.6 eV) tin disulfide (SnS_2).[14] The large bandgap of SnS_2 is advantageous to realize a high current on/off ratio with a suppressed dark current, besides extending the spectral range of photodetection.

2D materials have shown strong light–matter coupling caused by the sharp peaks in their density of states at certain energy levels thanks to the confinement effect.[15,16] Despite their strong interaction with incident photons, atomically thin 2D materials absorb a small portion of the incident light due to their optically transparent nature.[17] Likewise, the optical and optoelectronic performances of 2D materials based photodetectors are compromised.[18] To solve this issue, external photonic structures, such as optical cavities and waveguides, or metal NPs are integrated with 2D materials to improve their optical absorption.[19–21]

Here, we report the high performance and broadband photodetection of multilayer SnS_2 by decorating it with metal nanoparticles. Our results show that the decoration of silver nanoparticles (Ag-NPs) over SnS_2 channels leads to extended photodetection capabilities from UV to NIR (250–1050 nm). This is attributed to the localization of the electromagnetic field *via* the surface plasmon-enhanced optical field in the SnS_2 devices. In addition, we passivated the SnS_2/Ag-NPs devices with HfO_2, which demonstrated environmental stability with improved performance for more than seven weeks. Lastly, we demonstrated a flexible SnS_2/Ag-NPs device which retains ~80% of its photoresponsivity up to 500 bending cycles. Our results open possibilities for investigating wide band gap 2D semiconductors for broadband optoelectronic and photonic applications.

2. Results and discussion

2.1 SnS₂ FET

Figs. 1a and b show the device schematic with a circuit diagram and an optical microscopic image of the back-gated SnS_2 field-effect transistor (FET) on a Si/SiO₂ substrate, respectively. Before electrical measurements, we performed atomic force microscopy and Raman spectroscopy on the SnS_2 channel to ascertain its thickness and material quality, and the results are provided in ESI Fig. S1.† Our representative SnS_2 channel is ~13 nm thick, and it exhibits single Raman mode at ~316.4 cm^{-1} (A_{1g} mode), which is attributed to the relative vibration of Sn and S atoms in the out-of-plane direction.[22,23]

We performed the basic electrical measurements (transfer and output curves) on the multilayer SnS_2 FET in the dark, which is followed by an optoelectronic response under continuous wave lasers of different wavelengths. Note that all the measurements were performed under ambient conditions throughout this study. Fig. 1c shows the transfer curve obtained by sweeping the gate voltages (V_g) from −60 to +60 V at a constant bias voltage (V_{ds} = 0.5 V) under dark. The I_{ds}–V_g trend shows typical n-type (electron dominant) characteristics of the SnS_2 device, indicating that the Fermi level is positioned in the vicinity of the conduction band of SnS_2. Similar to MoS_2, the electron-rich characteristics in SnS_2 are attributed to the presence of sulfur vacancies and the strong Fermi level pinning effect close to the conduction band edge in SnS_2.[24,25] The device shows a current ON/OFF ratio of ~10³. From the slope of the transfer curve, *i.e.*, transconductance (g_m), we cal-
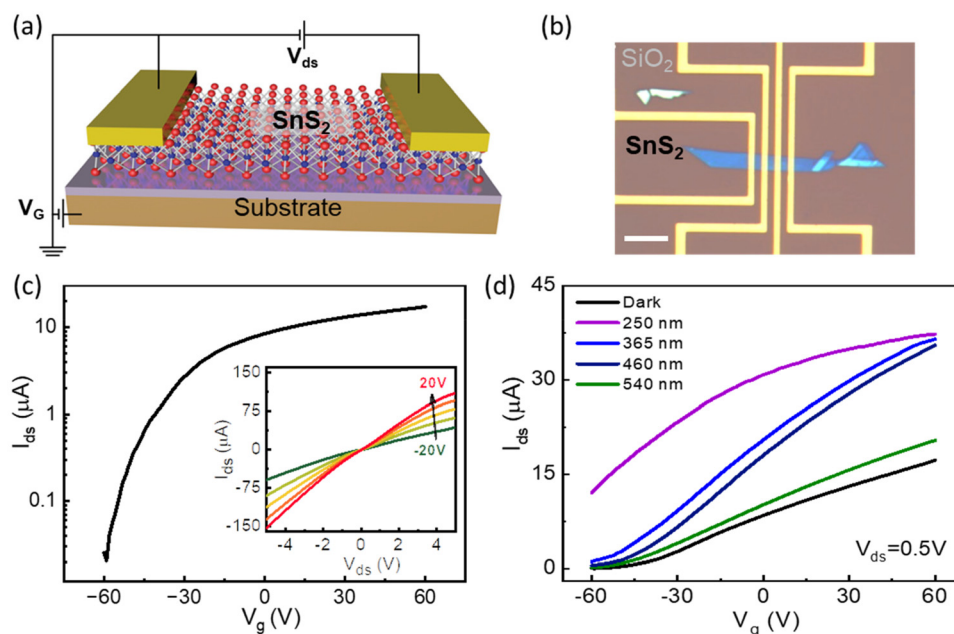

Fig. 1 Device architecture and electrical response of the SnS_2 FET. (a) Schematic diagram of the SnS_2 device. (b) Optical image of the back-gated SnS_2 device (L = 2 μm, W = 4.5 μm, and thickness = 13 nm) on a Si/SiO₂ substrate. Scale bar: 10 μm. (c) Current *vs.* back gate voltage (I_{ds}–V_g) plots in logarithmic scale at V_{ds} = 0.5 V. The inset shows the current *vs.* source-to-drain voltage (I_{ds}–V_{ds}) plots at V_g values ranging from −20 to 20 V with the step of 10 V. (d) I_{ds}–V_g trajectories of pristine SnS_2 under different light illuminations.

The extension in the detection range of the SnS_2 device to near IR is mainly caused by the enhanced and broadband optical absorption in the NPs-decorated SnS_2 devices.[30] We think that this enhancement is the combined effect of several factors.[31–33] First is the localized surface plasmon resonance (LSPR); the free electrons in Ag-NPs collectively oscillate at specific frequencies under illumination, leading to enhanced optical absorption and scattering by the NPs, and eventual enhancement in the photocurrent generation in SnS_2. The resonance frequencies depend on the size, shape, and wavelength of incident light, and can be studied in detail by employing finite element analysis in future. Second is light trapping; the Ag-NPs over the SnS_2 surface scatter the incident light, which is collected by neighboring NPs as plasmons instead of dissipating as free-space light, thus the strong optically interacting NPs trap light and increase the effective optical length and enhance the optical absorption, and hence an enhanced optoelectronic response in NPs-coacted SnS_2 device is observed. Third is the generation of hot electrons; the extinction of plasmons in the Ag-NPs may generate energetic, non-equilibrium charged carriers, also called hot electrons, which can be transferred to the SnS_2 surface, thus improving the photoresponsivity over a broad spectral range. We further compared the photodetector performances by estimating the rise and decay times of photodetectors from time-dependent photocurrent measurements. We obtained the rise and decay time responses by fitting the temporal photocurrent dataset, as shown in ESI Fig. S4,† by using eqn (2)

$$I_{ph} = I_{dark} + A\left(1 - e^{-\frac{t}{\tau_r}}\right) \quad \text{and} \quad I_{ph} = I_{dark} + Be^{\left(-\frac{t}{\tau_d}\right)} \quad (2)$$

where I_{ph} and I_{dark} are the photocurrent and dark current, respectively, A and B are the constants, and τ_r and τ_d denote the rise and decay times. For SnS_2, the average rise (8.1, 8.9, 8.5, and 7.8 s) and decay (19.9, 17.1, 15.8, 14.7 s) times were estimated at 250, 365, 460, and 540 nm wavelengths, respectively. Similarly, in the case of the Ag-NPs-decorated SnS_2 device, the average rise (7.1, 6.9, 7.3, and 6.1 s) and decay (15.8, 14.7, 12.0, 11.4 s) times were estimated at 250, 365, 460, and 540 nm wavelengths, respectively, as shown in Fig. 2d. Interestingly, a decrease in the rise and decay times is observed when SnS_2 is decorated with Ag-NPs. The Ag-NPs sustain the absorption of impurities, which can play a vital role in the reduction of response time.[34] The consistency of response times (rise/decay) at each wavelength indicates no significant alteration in the lifetime of the excited carriers.[35] To understand the role of traps or defect states in SnS_2 and the Ag-NPs-decorated SnS_2 photodetectors, we evaluated the optical power-dependent photoresponse. The trend of the photocurrent as per the power law has been reported to reveal the existence of trap states in a 2D channel.[36] By fitting Fig. 2e against the power law, i.e., $I_{ph} \propto AP^\vartheta$, we estimated ϑ values of 0.72 for SnS_2 and 0.58 for SnS_2/NPs. Note that the ϑ value closer to 1 indicates the existence of active low energy trap states and the ϑ value far from 1 indicates the active large energy trap states.[37] Therefore, these results indicate that the

trap states play a vital role in broadening the photodetection range in the SnS_2/NPs photodetectors. For example, the photogenerated carriers are trapped by the finite trap states, yielding the sub-linear dependence of the power-law formula of photocurrent.[38]

2.3 Passivated SnS_2/Ag-NPs/HfO_2 photodetector

Compared to other noble metal-based NPs, Ag-NPs are reported to be oxidized under ambient conditions, and this effect can be exaggerated under illumination conditions.[39] As a result, the performance of the Ag-NPs-coated SnS_2 device may degrade over time. To circumvent this, we deposited a ~15 nm thick high-k dielectric, HfO_2, by atomic layer deposition, as indicated in Fig. 3a schematic. The stabilities and performances of the pristine SnS_2, SnS_2/NPs, and SnS_2/Ag-NPs/HfO_2 devices were monitored under ambient conditions for the first seven weeks (Fig. 3b). For more details, see ESI S5 and S6.† Among these three different device configurations, SnS_2/Ag-NPs/HfO_2 demonstrated the highest photoresponsivity (R_{ph} = $I_{ph}/P_{op} \times A$; where P_{op} is the illuminated laser power and A is the active device area) of ~12 500 A W^{-1} at λ = 250 nm. Moreover, from the aging test result, we realized that the R_{ph} is reduced by ~20%, ~36%, and 6% for the SnS_2, SnS_2/Ag-NPs, and SnS_2/Ag-NPs/HfO_2 photodetectors after seven weeks under similar storage and operation conditions, as shown in Fig. 3c. This phenomenon is ascribed to the direct impact of oxygen on bare SnS_2, leading to the deterioration of material quality. In the case of SnS_2/Ag-NPs, the degradation is more pronounced due to surface oxidation and the consequent depreciation of the interface between SnS_2 and Ag-NPs. However, the introduction of HfO_2 passivation emerges as a pivotal mitigating factor. This passivation layer effectively impedes the interaction of oxygen with SnS_2 and Ag-NPs, thereby resulting in a mere 6% degradation and ensuring the stability of the devices with consistent performance. In a nutshell, the passivated SnS_2/Ag-NPs/HfO_2 photodetectors exhibit more stable performance for several weeks.

For further comparison among the three device configurations, we computed the external quantum efficiency (EQE = $hcR_{ph}/e\lambda$; where h is the Planck constant, c is the speed of light, and e is the elementary charge), which demonstrates the total electron–hole pair generation with the energy of one photon. The EQE was estimated to be ~8.7×10^5, ~2.4×10^6, and ~5.9×10^6% for SnS_2, SnS_2/NPs, and SnS_2/NPs/HfO_2, respectively. It is pertinent to note that our SnS_2/NPs/HfO_2 device exhibited superior EQE value compared to previous reports, which are summarized in Table 1.

2.4 Mechanical flexibility of the SnS_2/Ag-NPs photodetector

Among other advantages, 2D materials are mechanically robust, thus they can be incorporated for flexible applications. Therefore, we investigated the mechanical endurance of the Ag-NPs-coated SnS_2 photodetectors by bending polyethylene naphthalate (PEN) substrates with different radii, as shown schematically in Fig. 4a. The photoresponses as a function of time characteristics of the SnS_2/Ag-NPs photodetectors were
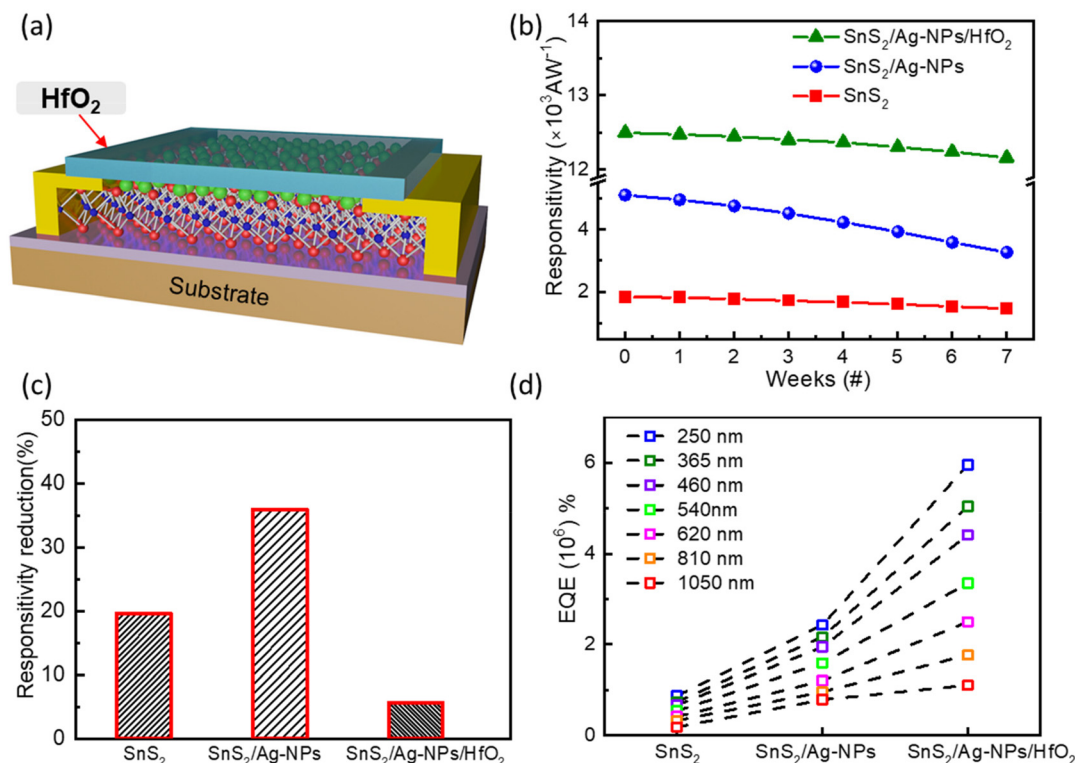
Fig. 3 Optoelectronic measurements of the HfO_2-passivated SnS_2/Ag-NPs device. (a) Schematic illustration of the HfO_2-passivated SnS_2/Ag-NPs device. (b) and (c) Comparison of the photoresponsibilities of SnS_2, SnS_2/Ag-NPs, and passivated SnS_2/Ag-NPs/HfO_2 photodetectors in first seven weeks in an ambient environment. (d) Comparison of the external quantum efficiencies of SnS_2, SnS_2/Ag-NPs, and passivated SnS_2/Ag-NPs/HfO_2 photodetectors at the given wavelengths of light.

Table 1 Summary of the key parameters of previous two-dimensional photodetectors

Material	Responsivity (A W^{-1})	Detectivity (Jones)	EQE (%)	Response time (rising, decay) sec	Ref.
SnS_2	300	6×10^9	4.6×10^4	36, 7	40
SnS_2	8.8×10^{-3}	10^9	24	0.005, 0.007	41
SnS_2	100	—	3.3×10^4	330, 130	42
SnS_2	2	—		42, 42	43
SnS_2	260	1.9×10^{10}	9.3×10^4	20, 16	44
SnS_2	1.19			1, 1	45
SnS_2	354	2×10^{10}	1.1×10^5	0.4, 0.5	46
MoS_2 Ag-NPs decorated	2.9×104			18, 7	47
SnS_2 Ag-NPs decorated	1.2×104	—	5.9×106	7, 16	This work

investigated at λ = 250 nm while holding the device at the bending position of various radii (0–flat, 20 mm, and 10 mm). Furthermore, we also illuminated at different light wavelengths (λ = 250, 540, and 1050 nm) at three different bending curvatures.

Fig. 4c depicts that the photoresponsivity of the flexible photodetector at 0 (flat), 20, and 10 mm was found to be ~4778, ~4575, and ~4332 A W^{-1} at λ = 250 nm, respectively. The results show that the photoresponse remains persistent at different curvature states, thereby indicating that the devices exhibit excellent mechanical flexibility and broadband photo-detection which are hardly affected by bending conditions. Moreover, the bending stability and reliability are the key factors of flexible photodetectors. Therefore, we bent (20 mm)

our devices several times and measured the endurance of the photocurrent. From Fig. 4d, it is observed that the photo-responsivity of the flexible photodetector is ~4556, ~4523, ~4101, and ~3561 after bending for 0, 50, 100, and 150 cycles, respectively. Importantly, after 150 cycles, the photo-responsivity of the device decreased by ~21%, which endorsed the photodetection stability of the flexible SnS_2/Ag-NPs device under multiple bending cycles of 20 mm curvature. Furthermore, to observe the mechanical stability we calculated the response time of flexible the SnS_2/Ag-NPs device at λ = 250 nm at various bending states. It is found that the response times are slightly reduced from 5.3 to 4.5 s (rise) and 6.7 to 6.1 s (decay) as the bending curvature is increased as shown in Fig. S8.† The reduction of response may be attributed to the
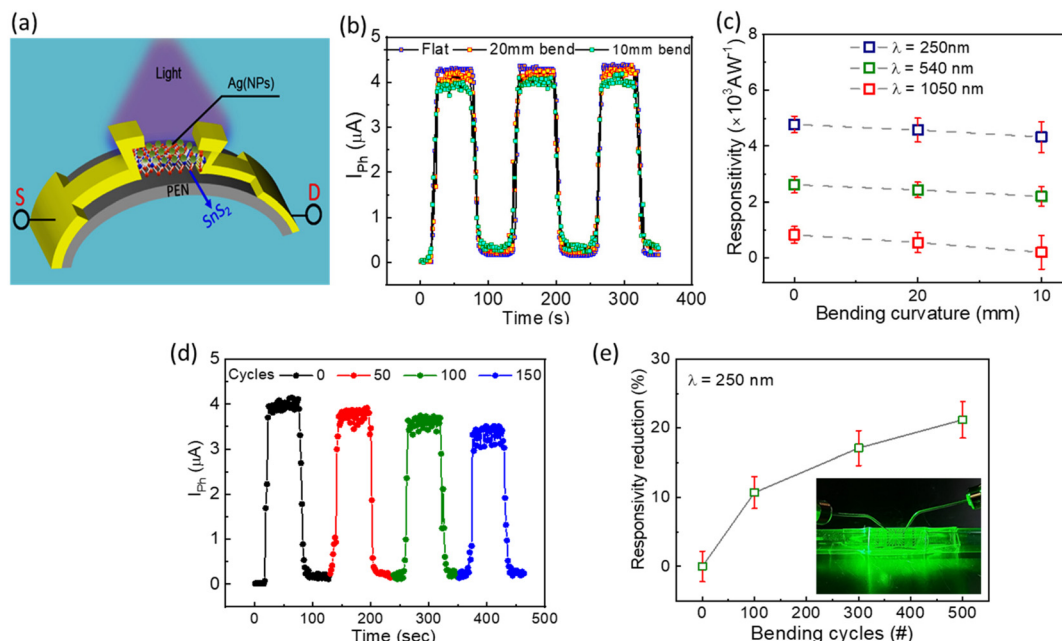
Fig. 4 Optoelectronic measurements of flexible SnS_2/Ag-NPs devices. (a) Schematic drawing of the flexible photodetector of SnS_2/Ag-NPs. (b) Temporal photoresponse of the flexible SnS_2/Ag-NP photodetector under the given bending curvatures at λ = 250 nm and P = 10 mW cm^{-2}. (c) Photoresponsivity of the flexible SnS_2/Ag-NPs photodetector at different wavelengths (λ = 250, 540, and 1050 nm). (d) Time-dependent photoresponse in different numbers of bending cycles. (e) Reduction of photoresponsivity of the SnS_2/Ag-NPs photodetector after various bending cycles. The bent radius was kept at 20 mm. The inset shows the flexible device in a bent position under light illumination.

defect states produced by stretching of the channel material SnS_2. However, the flexible measurements clearly exhibit repeated bending, making it an attractive material for wearable photodetectors.

3. Conclusion

In summary, we have reported multilayer SnS_2, SnS_2/Ag-NP, and SnS_2/Ag-NPs/HfO_2 transistors to elucidate the light–matter interaction for broadband photodetectors. The light sensing capabilities of SnS_2 are extended from the UV to near NIR (250–1050 nm) spectrum after decorating with Ag-NPs, which endorsed the extension of the cut-off wavelength in SnS_2. These results suggest the enhanced light absorption with localization of the electromagnetic field *via* the surface plasmon-enhanced optical field and the wide band gap of SnS_2 crystals. Furthermore, the photodetection performance, such as the photocurrent, photoresponsivity, and EQE, is significantly enhanced in the passivated Ag-NP-decorated SnS_2 devices when compared to the bare SnS_2 devices. In addition, we estimated the photo-performance deterioration of each device, where it was found that the SnS_2/Ag-NPs/HfO_2 device showed excellent stability with a meager reduction in photoresponsivity as compared to other devices. Moreover, we made a flexible SnS_2/Ag-NPs photodetector, which showed a broadband light response having stability up to 500 bending cycles at a 20 mm curvature. Thus, our results provide an efficient

approach to extend the optical and flexible sensing capabilities in wide bandgap 2D materials from UV to NIR for multifunctional photoelectronic devices.

4. Materials and methods

To make large-scale patterns on Si/SiO_2 substrates, we first performed photolithography. The chips were sonicated in acetone and isopropanol solvents, and later rinsed with piranha solution and washed with de-ionized water for 15 minutes to ensure the proper removal of contamination from the Si/SiO_2 chips. The chips were soft-baked in a furnace at 125 °C to remove moisture. The 2D crystals of SnS_2 were physically peeled off from the bulk crystals using a scotch tape and transferred to pre-patterned Au contact pads on Si/SiO_2 wafers by the dry transfer method using the polydimethylsiloxane (PDMS) stamp technique. We used atomic force microscopy (AFM), XE-100 by Park Systems Inc., for precise thickness measurements of the SnS_2 flakes. Subsequently, we performed electron beam lithography (EBL) to pattern metal electrodes. After EBL, we evaporated the Cr and Au metals of 5 and 80 nm thick, respectively, for metallization of the electrodes. Finally, the devices were immersed in acetone to lift-off the excess metal from the substrate. In addition, for flexible measurements, we used polyethylene naphthalate (PEN) substrates to fabricate the SnS_2/Ag-NPs photodetector. Raman spectroscopy (Renishaw, In Via systems) was performed with a laser source

of 514 nm under ambient conditions. Furthermore, atomic layer deposition (ALD) was used to deposit HfO_2 (~15 nm) at 250 °C at a rate of 0.1 nm per cycle. Electrical measurements were performed by employing a voltmeter (Keithley 2400) and a picoammeter (Keithley 6485).

Conflicts of interest

All authors have no conflict to declare.

Acknowledgements

References

1 O. Lopez-Sanchez, D. Lembke, M. Kayci, A. Radenovic and A. Kis, Ultrasensitive Photodetectors Based on Monolayer MoS_2, *Nat. Nanotechnol.*, 2013, **8**(7), 497–501.

2 X. Wang, D. Pan, M. Sun, F. Lyu, J. Zhao and Q. Chen, High-Performance Room-Temperature UV-IR Photodetector Based on the InAs Nanosheet and Its Wavelength- and Intensity-Dependent Negative Photoconductivity, *ACS Appl. Mater. Interfaces*, 2021, **13**(22), 26187–26195.

3 Y. Chen, W. Ma, C. Tan, M. Luo, W. Zhou, N. Yao, H. Wang, L. Zhang, T. Xu, T. Tong, Y. Zhou, Y. Xu, C. Yu, C. Shan, H. Peng, F. Yue, P. Wang, Z. Huang and W. Hu, Broadband Bi_2O_2Se Photodetectors from Infrared to Terahertz, *Adv. Funct. Mater.*, 2021, **31**(14), 2009554.

4 O. Ozturk, B. M. Candan, S. Kurnaz, O. Cicek and A. T. Tasci, Solar Light Performances of N-ZnO Nanorods/p-Si-Based Photodetectors under High Illumination Intensity, *J. Mater. Sci.: Mater. Electron.*, 2022, **33**(18), 15222–15231.

5 A. Castellanos-Gomez, V. Singh, H. S. J. van der Zant and G. A. Steele, Mechanics of Freely-Suspended Ultrathin Layered Materials, *Ann. Phys.*, 2015, **527**(1–2), 27–44.

6 H. Chen, H. Liu, Z. Zhang, K. Hu and X. Fang, Nanostructured Photodetectors: From Ultraviolet to Terahertz, *Adv. Mater.*, 2016, **28**(3), 403–433.

7 S. Kaushik and R. Singh, 2D Layered Materials for Ultraviolet Photodetection: A Review, *Adv. Opt. Mater.*, 2021, **9**(11), 2002214.

8 Z. Wang, Q. Tu, S. Zheng, J. J. Urban, S. Li and B. Mi, Understanding the Aqueous Stability and Filtration Capability of MoS_2 Membranes, *Nano Lett.*, 2017, **17**(12), 7289–7298.

9 M. P. Ulmer, Future UV Detectors for Space Applications, *Proc. SPIE, Optical Sensing II*, 2006, **6189**, 1–10.

10 M. Kaliszewski, M. Włodarski, A. Bombalska, M. Kwaśny, M. Mularczyk-Oliwa, J. Młyńczak and K. Kopczyński, The Application of Semiconductor Based UV Sources for the Detection and Classification of Biological Material, *Proc. SPIE, Laser Tech 2012: Applications for Laser*, 2013, **8703**, 24–31.

11 J. Kaur, M. Singh, C. Dell'Aversana, R. Benedetti, P. Giardina, M. Rossi, M. Valadan, A. Vergara, A. Cutarelli, A. M. I. Montone, L. Altucci, F. Corrado, A. Nebbioso and C. Altucci, Biological Interactions of Biocompatible and Water-Dispersed MoS_2 Nanosheets with Bacteria and Human Cells, *Sci. Rep.*, 2018, **8**(1), 16386.

12 L. Huang, A. Krasnok, A. Alú, Y. Yu, D. Neshev and A. E. Miroshnichenko, Enhanced Light–Matter Interaction in Two-Dimensional Transition Metal Dichalcogenides, *Rep. Prog. Phys.*, 2022, **85**(4), 046401.

13 A. Castellanos-Gomez, Black Phosphorus: Narrow Gap, Wide Applications, *J. Phys. Chem. Lett.*, 2015, **6**(21), 4280–4291.

14 E. V. Rusu, N. N. Syrbu, A. V. Tiron and V. V. Zalamai, Band Structure and Optical Constants of SnS_2 Single Crystals, *Mater. Res. Express*, 2019, **6**(4), 046203.

15 L. Du, T. Hasan, A. Castellanos-Gomez, G.-B. Liu, Y. Yao, C. N. Lau and Z. Sun, Engineering Symmetry Breaking in 2D Layered Materials, *Nat. Rev. Phys.*, 2021, **3**, 193–206.

16 L. Britnell, R. M. Ribeiro, A. Eckmann, R. Jalil, B. D. Belle, A. Mishchenko, Y. J. Kim, R. V. Gorbachev, T. Georgiou, S. V. Morozov, A. N. Grigorenko, A. K. Geim, C. Casiraghi, A. H. C. Neto and K. S. Novoselov, Strong Light-Matter Interactions in Heterostructures of Atomically Thin Films, *Science*, 2013, **340**(6138), 1311–1314.

17 C. Hsu, R. Frisenda, R. Schmidt, A. Arora, S. M. Vasconcellos, R. Bratschitsch, H. S. J. Zant and A. Castellanos-Gomez, Thickness–Dependent Refractive Index of 1L, 2L, and 3L MoS_2, $MoSe_2$, WS_2, and WSe_2, *Adv. Opt. Mater.*, 2019, **7**(13), 1900239.

18 X. Jia, C. Tang, R. Pan, Y. Long, C. Gu and J. Li, Thickness-Dependently Enhanced Photodetection Performance of Vertically Grown SnS_2 Nanoflakes with Large Size and High Production, *ACS Appl. Mater. Interfaces*, 2018, **10**(21), 18073–18081.

19 M. F. Khan, S. Rehman, I. Akhtar, S. Aftab, H. M. S. Ajmal, W. Khan, D. Kim and J. Eom, High Mobility $ReSe_2$ Field Effect Transistors: Schottky-Barrier-Height-Dependent Photoresponsivity and Broadband Light Detection with Co Decoration, *2D Mater.*, 2019, **7**(1), 015010.

20 S. Latini, E. Ronca, U. De Giovannini, H. Hübener and A. Rubio, Cavity Control of Excitons in Two-Dimensional Materials, *Nano Lett.*, 2019, **19**(6), 3473–3479.

21 S. Parhizkar, M. Prechtl, A. L. Giesecke, S. Suckow, S. Wahl, S. Lukas, O. Hartwig, N. Negm, A. Quellmalz, K. Gylfason, D. Schall, M. Wuttig, G. S. Duesberg and M. C. Lemme, Two-Dimensional Platinum Diselenide Waveguide-Integrated Infrared Photodetectors, *ACS Photonics*, 2022, **9**(3), 859–867.

22 Y. Ding, W. Zheng, X. Lu, Y. Liang, Y. Zhu, M. Jin and F. Huang, Raman Tensor of Layered SnS$_2$, *J. Phys. Chem. Lett.*, 2020, **11**(23), 10094–10099.

23 T. Sriv, K. Kim and H. Cheong, Low-Frequency Raman Spectroscopy of Few-Layer 2H-SnS2, *Sci. Rep.*, 2018, **8**(1), 10194.

24 P. Bampoulis, R. van Bremen, Q. Yao, B. Poelsema, H. J. W. Zandvliet and K. Sotthewes, Defect Dominated Charge Transport and Fermi Level Pinning in MoS$_2$/Metal Contacts, *ACS Appl. Mater. Interfaces*, 2017, **9**(22), 19278–19286.

25 D. Liu, Y. Guo, L. Fang and J. Robertson, Sulfur Vacancies in Monolayer MoS$_2$ and Its Electrical Contacts, *Appl. Phys. Lett.*, 2013, **103**(18), 183113.

26 M. F. Khan, F. Ahmed, S. Rehman, I. Akhtar, M. A. Rehman, P. A. Shinde, K. Khan, D. Kim, J. Eom, H. Lipsanen and Z. Sun, High Performance Complementary WS$_2$ Devices with Hybrid Gr/Ni Contacts, *Nanoscale*, 2020, **12**(41), 21280–21290.

27 S. Malynych and G. Chumanov, Light-Induced Coherent Interactions between Silver Nanoparticles in Two-Dimensional Arrays, *J. Am. Chem. Soc.*, 2003, **125**(10), 2896–2898.

28 B. Sun, Z. Wang, Z. Liu, X. Tan, X. Liu, T. Shi, J. Zhou and G. Liao, Tailoring of Silver Nanocubes with Optimized Localized Surface Plasmon in a Gap Mode for a Flexible MoS$_2$ Photodetector, *Adv. Funct. Mater.*, 2019, **29**(26), 1900541.

29 D. Mouloua, M. El Marssi, M. A. El Khakani and M. Jouiad, Enhanced photodetection properties of CVD-grown MoS$_2$ nanosheets onto Ag-nanoparticles decorated substrates, in *IEEE EUROCON 2023–20th International Conference on Smart Technologies*, IEEE, Torino, Italy, 2023, pp. 138–141. DOI: 10.1109/EUROCON56442.2023.10199014.

30 R. Liu, F. Wang, L. Liu, X. He, J. Chen, Y. Li and T. Zhai, Band Alignment Engineering in Two-Dimensional Transition Metal Dichalcogenide-Based Heterostructures for Photodetectors, *Small Struct.*, 2021, **2**(3), 2000136.

31 L. Chang, L. V. Besteiro, J. Sun, E. Y. Santiago, S. K. Gray, Z. Wang and A. O. Govorov, Electronic Structure of the Plasmons in Metal Nanocrystals: Fundamental Limitations for the Energy Efficiency of Hot Electron Generation, *ACS Energy Lett.*, 2019, **4**(10), 2552–2568.

32 Y. Li, W. Shi, A. Gupta and N. Chopra, Morphological Evolution of Gold Nanoparticles on Silicon Nanowires and Their Plasmonics, *RSC Adv.*, 2015, **5**(61), 49708–49718.

33 C. V. Hoang, K. Hayashi, Y. Ito, N. Gorai, G. Allison, X. Shi, Q. Sun, Z. Cheng, K. Ueno, K. Goda and H. Misawa, Interplay of Hot Electrons from Localized and Propagating Plasmons, *Nat. Commun.*, 2017, **8**(1), 771.

34 W. Jing, N. Ding, L. Li, F. Jiang, X. Xiong, N. Liu, T. Zhai and Y. Gao, Ag Nanoparticles Modified Large Area Monolayer MoS$_2$ Phototransistors with High Responsivity, *Opt. Express*, 2017, **25**(13), 14565–14574.

35 J. Pak, I. Lee, K. Cho, J. K. Kim, H. Jeong, W. T. Hwang, G. H. Ahn, K. Kang, W. J. Yu, A. Javey, S. Chung and T. Lee, Intrinsic Optoelectronic Characteristics of MoS$_2$ Phototransistors via a Fully Transparent van der Waals Heterostructure, *ACS Nano*, 2019, **13**(8), 9638–9646.

36 H. Fang and W. Hu, Photogating in Low Dimensional Photodetectors, *Adv. Sci.*, 2017, **4**(12), 1700323.

37 Y. Wang, X. Huang, D. Wu, R. Zhuo, E. Wu, C. Jia, Z. Shi, T. Xu, Y. Tian and X. Li, A Room-Temperature near-Infrared Photodetector Based on a MoS$_2$/CdTe p–n Heterojunction with a Broadband Response up to 1700 nm, *J. Mater. Chem. C*, 2018, **6**(18), 4861–4865.

38 G. Wu, X. Wang, Y. Chen, Z. Wang, H. Shen, T. Lin, W. Hu, J. Wang, S. Zhang, X. Meng and J. Chu, Ultrahigh Photoresponsivity MoS$_2$ Photodetector with Tunable Photocurrent Generation Mechanism, *Nanotechnology*, 2018, **29**(48), 485204.

39 N. Grillet, D. Manchon, E. Cottancin, F. Bertorelle, C. Bonnet, M. Broyer, J. Lermé and M. Pellarin, Photo-Oxidation of Individual Silver Nanoparticles: A Real-Time Tracking of Optical and Morphological Changes, *J. Phys. Chem. C*, 2013, **117**(5), 2274–2282.

40 X. Zhou, L. Gan, Q. Zhang, X. Xiong, H. Li, Z. Zhong, J. Han and T. Zhai, High Performance Near-Infrared Photodetectors Based on Ultrathin SnS Nanobelts Grown via Physical Vapor Deposition, *J. Mater. Chem. C*, 2016, **4**(11), 2111–2116.

41 G. Su, V. G. Hadjiev, P. E. Loya, J. Zhang, S. Lei, S. Maharjan, P. Dong, P. M. Ajayan, J. Lou and H. Peng, Chemical Vapor Deposition of Thin Crystals of Layered Semiconductor SnS$_2$ for Fast Photodetection Application, *Nano Lett.*, 2015, **15**(1), 506–513.

42 Y. Huang, H. Deng, K. Xu, Z. Wang, Q. Wang, F. Wang, F. Wang, X. Zhan, S. Li, J. Luo and J. He, Highly sensitive and fast phototransistor based on large size CVD-grown SnS$_2$ nanosheets, *Nanoscale*, 2015, **7**, 14093–14099.

43 J. Xia, D. Zhu, L. Wang, B. Huang, X. Huang and X.-M. Meng, Large-Scale Growth of Two-Dimensional SnS$_2$ Crystals Driven by Screw Dislocations and Application to Photodetectors, *Adv. Funct. Mater.*, 2015, **25**(27), 4255–4261.

44 X. Zhou, Q. Zhang, L. Gan, H. Li and T. Zhai, Large–Size Growth of Ultrathin SnS$_2$ Nanosheets and High Performance for Phototransistors, *Adv. Funct. Mater.*, 2016, **26**, 4405–4413.

45 D. Yang, B. Li, C. Hu, H. Deng, D. Dong, X. Yang, K. Qiao, S. Yuan and H. Song, Controllable Growth Orientation of

SnS$_2$ Flakes for Low-Noise, High-Photoswitching Ratio, and Ultrafast Phototransistors, *Adv. Opt. Mater.*, 2016, **4**(3), 419–426.

46 X. Jia, C. Tang, R. Pan, Y. Long, C. Gu and J. Li, Thickness-Dependently Enhanced Photodetection Performance of Vertically Grown SnS$_2$ Nanoflakes with Large Size and High Production, *ACS Appl. Mater. Interfaces*, 2018, **10**(21), 18073–18081.

47 W. Jing, N. Ding, L. Li, F. Jiang, X. Xiong, N. Liu, T. Zhai and Y. Gao, Ag Nanoparticles Modified Large Area Monolayer MoS$_2$ Phototransistors with High Responsivity, *Opt. Express*, 2017, **25**(13), 14565–14574.